
Message-Passing Monte Carlo: Generating low-discrepancy point sets via Graph Neural Networks

Anonymous Authors¹

Abstract

Discrepancy is a well-known measure for the irregularity of the distribution of a point set. Point sets with small discrepancy are called low-discrepancy and are known to efficiently fill the space in a uniform manner. Low-discrepancy points play a central role in many problems in science and engineering, including numerical integration, computer vision, machine perception, computer graphics, machine learning, and simulation. In this work, we present the first machine learning approach to generate a new class of low-discrepancy point sets named *Message-Passing Monte Carlo (MPMC)* points. Motivated by the geometric nature of generating low-discrepancy point sets, we leverage tools from Geometric Deep Learning and base our model on Graph Neural Networks. We further provide an extension of our framework to higher dimensions, which flexibly allows the generation of custom-made points that emphasize the uniformity in specific dimensions that are primarily important for the particular problem at hand. Finally, we demonstrate that our proposed model achieves state-of-the-art performance superior to previous methods by a significant margin. In fact, MPMC points are empirically shown to be either optimal or near-optimal with respect to the discrepancy for every dimension and the number of points for which the optimal discrepancy can be determined.

1. Introduction

Monte Carlo (MC) methods have been commonly used and are a popular choice for approximating and simulating complex real-world systems. Known for their reliance on repeated random sampling, MC methods function well in

¹Anonymous Institution, Anonymous City, Anonymous Region, Anonymous Country. Correspondence to: Anonymous Author <anon.email@domain.com>.

Preliminary work. Under review at ICML 2024 AI for Science workshop. Do not distribute.

problems involving optimization, numerical integration, and financial mathematics (particularly derivative pricing and risk management) via computer simulation. However, their convergence rate of $\mathcal{O}(N^{-1/2})$ in the number of samples N means that achieving high precision with MC requires an impractically large number of samples for complex problems. To address this drawback, it is common to employ *variance reduction techniques* such as importance sampling, stratified sampling, or control of variates to obtain the same degree of accuracy with fewer samples (for details, see (Glasserman, 2004), (Lemieux, 2009) and references therein).

A particularly successful approach for convergence is called *quasi-Monte Carlo (QMC)*. QMC methods employ a deterministic point set, which replaces the purely random sampling with a sample whose points span the hypercube $[0, 1]^d$ in a manner that is more uniform than what can be achieved with MC sampling. The fact that these point sets are constructed over $[0, 1]^d$ is not overly restrictive as most, if not all, sampling algorithms used within the MC method take as input (pseudo)random numbers in $[0, 1]$. The uniformity of these deterministic point sets (or indeed, any point set) can be captured by one of several of measures of irregularity of distribution, referred to by the umbrella term *discrepancy measures* (Drmotá & Tichý, 1997). The more uniformly distributed the points are, the lower the discrepancy is; point sets possessing a small enough discrepancy value are called *low-discrepancy*. In the classical setting, the *star-discrepancy*, widely regarded as the most important uniformity measure, of an N -element point set $\{\mathbf{X}_i\}_{i=1}^N$ contained in $[0, 1]^d$ represents the largest absolute difference between the volume of a test box and the proportion of points of $\{\mathbf{X}_i\}_{i=1}^N$ that fall inside the test box,

$$D^* (\{\mathbf{X}_i\}_{i=1}^N) := \sup_{\mathbf{x} \in [0, 1]^d} \left| \frac{\# (\{\mathbf{X}_i\}_{i=1}^N \cap [0, \mathbf{x}])}{N} - \mu([0, \mathbf{x}]) \right| \quad (1)$$

where $\# (\{\mathbf{X}_i\}_{i=1}^N \cap [0, \mathbf{x}])$ counts how many points of $\{\mathbf{X}_i\}_{i=1}^N$ fall inside the box $[0, \mathbf{x}] = \prod_{i=1}^d [0, x_i]$ for $\mathbf{x} = (x_1, \dots, x_d) \in [0, 1]^d$, and $\mu(\cdot)$ denotes the usual Lebesgue measure. Despite the framing in (1), computation of the star-discrepancy is known to be a discrete problem; see (Niederreiter, 1972). The discrepancy is closely re-

lated to worst-case integration error of a particular class of functions with the most well-known result being the Koksma-Hlawka inequality; see (Kuipers & Niederreiter, 1974; Hlawka, 1984). Explicitly, given a point set $\{\mathbf{X}_i\}_{i=1}^N$ contained in $[0, 1]^d$, we have

$$\left| \int_{[0,1]^d} f(\mathbf{x})d\mathbf{x} - \frac{1}{N} \sum_{i=1}^N f(\mathbf{X}_i) \right| \leq D^*(\{\mathbf{X}_i\}_{i=1}^N)V(f) \tag{2}$$

where $V(f)$ denotes the variation of the function f in the sense of Hardy and Krause. This result illustrates that points with small discrepancy induce approximations with small errors. Thus in summary, it is of general interest to find N -point configurations with smallest discrepancy; see (Cauwet et al., 2020; Galanti & Jung, 1997; Paulin et al., 2022; Mishra & Rusch, 2021; Longo et al., 2021) for examples of QMC implementation.

Given this context, our main goal is to present a machine learning framework that generates point sets with minimal discrepancy. Based on the geometric nature of this problem, we suggest to leverage graph-learning models from Geometric Deep Learning (Bronstein et al., 2021) to achieve this. More concretely, we construct a computational graph based on nearest neighbors of the initial input points and process the encoded input points with a deep message-passing neural network, which is trained to minimize a closed-form solution of a specific discrepancy measure of its decoded and clamped outputs. We term the resulting low-discrepancy points **Message-Passing Monte Carlo (MPMC)** points. While previous methods are either far from obtaining optimal discrepancy values or intractable to compute (and thus are only available in $d = 2, 3$ and very small number of points $N \leq 20$), MPMC reaches near-optimal discrepancy in near-real time for potentially thousands of points. This advancement represents a significant step forward in the development of highly efficient sampling methods, which are crucial for many applications in science and engineering. Concrete examples include problems in financial mathematics (L’Ecuyer, 2009), path and motion planning in robotics (Branicky et al., 2001), and enhanced training of 3-D computer-vision models like Neural Radiance Fields (NeRFs) (Mildenhall et al., 2021).

Main contributions. In the subsequent sections, we will:

- introduce a new state-of-the-art machine learning model that generates low-discrepancy points. To our knowledge, this is the first machine learning approach in this context.
- extend our framework to higher dimensions by minimizing the average discrepancy of randomly selected subsets of projections. This allows for generating

custom-made points that emphasize specific dimensions that are primarily important for the particular problem at hand.

- provide an extensive empirical evaluation of our proposed MPMC point sets and demonstrate their superior performance over previous methods.

2. Background and previous work

Our general goal in this paper is to provide a method for generating point sets with small discrepancy. In the following, we use the term *sequence* to refer to an infinite series of points, and *point set* for a finite one. Both these objects are closely related as many results on sequences in dimension d correspond to those on sets in dimension $d + 1$; see (Roth, 1954).

A sequence of points $\{\mathbf{X}_i\}_{i=1}^\infty$ contained in $[0, 1]^d$ is called a low-discrepancy sequence if the star-discrepancy of the first N points satisfies $D^*(\{\mathbf{X}_i\}_{i=1}^N) = \mathcal{O}((\log N)^d/N)$. A finite point set $\{\mathbf{X}_i\}_{i=1}^N$ is said to be of low discrepancy if its corresponding star-discrepancy $D^*(\{\mathbf{X}_i\}_{i=1}^N)$ is “small” enough, which in practice means that a bound of the form $c(\log N)^{d-1}/N$ can be established, for a given constant c independent of N (but possibly dependent on d). Moving forward, for comparison purposes, we will regularly truncate various known infinite low-discrepancy sequences resulting in a finite point set, which inherits the low-discrepancy property from the underlying infinite sequence.

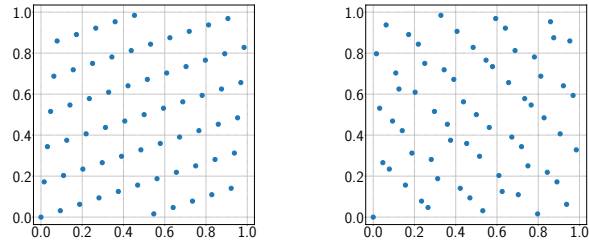


Figure 1. Two different low-discrepancy point sets with $N = 64$: Korobov lattice (left), and Sobol’ (right).

Figure 1 illustrates two examples of low-discrepancy point sets. On the left-hand side we have a Korobov lattice (Korobov, 1963), which is an example of a lattice rule (Haber, 1970; Sloan & Joe, 1994; Nuyens, 2014; Dick et al., 2022), and on the right-hand side, we see the first 64 points of the two-dimensional Sobol’ sequence (Sobol’, 1967). This construction leverages a widely used building block for many low-discrepancy sequences known as the van der Corput sequence in base b (van der Corput, 1935). It is also an example of what are modernly known as digital (t, s) -sequences—which also include the Faure sequences (Faure, 1982)—that were first laid out in (Niederreiter, 1987), with a

comprehensive overview provided in the subsequent monograph (Niederreiter, 1992). Halton sequences (Halton, 1960) are another widely used type of low-discrepancy sequences that concatenate d van der Corput sequences in different bases, usually taken as the first d prime numbers.

More recently, there have been successful attempts to construct low-discrepancy point sets using more sophisticated means motivated by the lack of constructions adapted to specific N and d . In (Doerr & De Rainville, 2013), new low-discrepancy point sets were suggested via the optimization of permutations applied to a Halton sequence. As a consequence, several open problems were solved regarding sets with small discrepancy from (Novak & Woźniakowski, 2010). Further, in (Doerr et al., 2005) an algorithm for constructing a low-discrepancy set via a derandomized version of Hoeffding’s inequality was provided which was shown to improve the previous best known upper bounds for the star-discrepancy. As some of the most recent work in this direction, a method called *subset selection* was presented in (Clément et al., 2022; 2024) to choose from an N -element point set (in practise, usually the first N points of the Sobol’ sequence) the $k < N$ points which yield the smallest discrepancy using a swap-based heuristic. Furthermore, a method to generate optimal star-discrepancy point sets for fixed N and d based on a non-linear programming approach was suggested in (Clément et al., 2023). However, this formulation of the problem presented huge computational burdens allowing optimal sets only to be found up to 20 points in dimension two and 8 points in dimension three.

3. Method

Let $1 < d < +\infty$ and $1 \leq N < +\infty$ be fixed natural numbers. Our objective is to train a neural network to transform (random) input points $\{\mathbf{X}_i\}_{i=1}^N$ into points $\{\hat{\mathbf{X}}_i\}_{i=1}^N$ that reduce the star-discrepancy $D^*(1)$, where $\mathbf{X}_i, \hat{\mathbf{X}}_i \in [0, 1]^d$ for all i .

In this work, we propose to leverage Graph Neural Networks (GNNs) (Sperduti, 1994; Goller & Kuchler, 1996; Sperduti & Starita, 1997; Frasconi et al., 1998; Gori et al., 2005; Scarselli et al., 2008; Bruna et al., 2014; Defferrard et al., 2016; Kipf & Welling, 2017; Monti et al., 2017) based on the message-passing framework to effectively learn such transformations. GNNs are a popular class of model architectures for learning on relational data, and have successfully been applied on a variety of different tasks, e.g., in computer science (Monti et al., 2017; Derrow-Pinion et al., 2021; Ying et al., 2018), and the natural sciences (Gilmer et al., 2017; Gaudelot et al., 2021; Shlomi et al., 2020) (see (Zhou et al., 2019; Bronstein et al., 2021) for additional applications). In particular, GNNs have successfully been used in the context of learning on point clouds, or generally learning on sets. This motivates the choice of GNNs in our

setup, where specific transformations of geometric sets (i.e., set of input points in $[0, 1]^d$) have to be learned.

A schematic drawing of our approach can be seen in Fig. 2, where we train a GNN model to transform $N = 64$ random input points $\{\mathbf{X}_i\}_{i=1}^N$ into low-discrepancy points $\{\hat{\mathbf{X}}_i\}_{i=1}^N$.

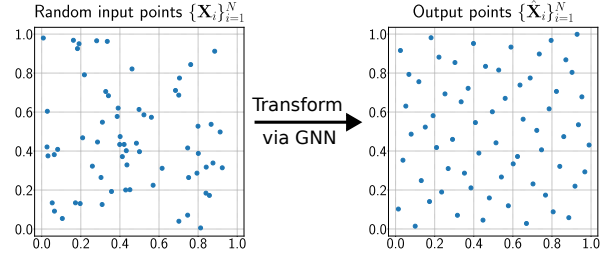


Figure 2. Schematic drawing of our proposed approach to transform (random) input points $\{\mathbf{X}_i\}_{i=1}^N$ into low-discrepancy points $\{\hat{\mathbf{X}}_i\}_{i=1}^N$. Both the input and output point sets are actual instances of our proposed model, with $N = 64$ and $d = 2$ in this example.

3.1. Training set

Our approach can be classified as an unsupervised learning setup, where, in contrast to supervised learning, only input data is required without any labels. While it is intuitive to generate the set of input points randomly, we suggest several different approaches for constructing input data:

1. Uniform random sampled set of input points: $\mathbf{X}_i \sim \mathcal{U}([0, 1]^d)$, for all points $i = 1, \dots, N$.
2. Base set of input points from available low-discrepancy point sets, such as Sobol’, Halton, or a lattice rule.
3. Base set of input points from randomly perturbed low-discrepancy points, i.e.,

$$\mathbf{X}_i = \mathbf{Y}_i + \xi \pmod{1}, \quad (3)$$

where \mathbf{Y}_i is generated by a known low-discrepancy sequence and ξ is uniform randomly sampled from $[0, b]^d$, with $0 < b \leq 1$, for all points $i = 1, \dots, N$.

3.2. Architecture

Let $\mathcal{G} = (\mathcal{V}, \mathcal{E} \subseteq \mathcal{V} \times \mathcal{V})$ be an undirected, connected graph with $|\mathcal{V}| = N$ nodes and $|\mathcal{E}| = e$ edges (unordered pairs of nodes $\{i, j\}$ denoted $i \sim j$). We further denote the 1 -neighborhood of a node $i \in \mathcal{V}$ as $\mathcal{N}_i = \{j \in \mathcal{V} : i \sim j\}$. In addition, each node $i \in \mathcal{V}$ is equipped with an m -dimensional feature vector $\mathbf{X}_i \in \mathbb{R}^m$. The main building block of our model consist of GNN layers based on the message-passing framework. This family of parametric functions is defined through local updates of hidden node

representations. More concretely, we iteratively update node features as,

$$\mathbf{X}_i^l = \phi^l \left(\mathbf{X}_i^{l-1}, \bigoplus_{j \in \mathcal{N}_i} \psi^l(\mathbf{X}_i^{l-1}, \mathbf{X}_j^{l-1}) \right), \forall l = 1, \dots, L, \quad (4)$$

where \bigoplus denotes a permutation-invariant operation, such as SUM, MEAN, or MAX, and $\mathbf{X}_i^l \in \mathbb{R}^{m_l}$ for all nodes i . Moreover, we parameterize ϕ^l, ψ^l as ReLU-multilayer perceptrons (MLPs), i.e., MLPs using the element-wise $\text{ReLU}(x) = \max(0, x)$ activation function in-between layers. We further encode the initial node features by a transformation that maps the initial points in dimension d to our initial hidden node feature dimension m_0 . Moreover, we decode the output of the final GNN layer by a transformation that maps the hidden node features of dimension m_L back to the physical dimension d . Both the encoder as well as the decoder are parameterized as affine transformations. Finally, we smoothly clamp the decoded outputs back into $[0, 1]^d$ by using the element-wise sigmoidal activation function,

$$\text{sigmoid}(x) = \frac{1}{1 + e^{-x}}.$$

Note that this step is crucial, as otherwise the training objectives we introduce in the subsequent sections are ill-defined. Moreover, the clamping step has to be differentiable in order to be used within a gradient-based learning framework.

Another important part of the GNN architecture is the construction of the underlying computational graph \mathcal{G} , i.e., defining the local structure \mathcal{N}_i for all nodes i in (4). It is worth noting that in many GNN applications (e.g., network science, or life sciences) the computational graph is already given a-priori, either explicitly or implicitly. In contrast to that, our problem setup considers the construction of the underlying computational graph as an additional design choice. While there are many suitable choices, often balancing a global vs local connectivity structure, we suggest to construct the underlying graph \mathcal{G} based on nearest neighbors, i.e., for a fixed radius $0 < r \leq 1$,

$$\mathcal{N}_i = \{j \in \mathcal{V} : \|\mathbf{X}_i - \mathbf{X}_j\|_2 \leq r\}. \quad (5)$$

We choose this inherently local structure to guide the GNN training towards transforming input points into low-discrepancy points by mainly considering the positions of other near-by points (in the corresponding Euclidean space of the input point set). A schematic of the full model can be seen in Fig. 3.

3.3. Training objective

Our ultimate goal is to minimize the star-discrepancy D^* (1). However, D^* cannot serve as the training objective, as (i) D^* is computationally infeasible to calculate for high

dimensions d and large number of points N (it has been shown to be an NP-hard problem in (Gnewuch et al., 2009) and in fact, it is even $W[1]$ -hard in d (Giannopoulos et al., 2012)); (ii) the training objective should not only be computationally feasible but rather very efficient to compute, as it needs to be evaluated at every step of the training procedure (i.e., for every step of the gradient descent method) resulting in potentially thousands of evaluations to train only a single model, and (iii) the training objective needs to be differentiable in order to be used in the context of gradient-based learning. It turns out, we can derive a training objective resolving all three issues while simultaneously minimizing D^* by leveraging previous work on the \mathcal{L}_p -discrepancy,

$$\mathcal{L}_p(\{\mathbf{X}_i\}_{i=1}^N) := \left(\int_{[0,1]^d} \left| \frac{\#\{\mathbf{X}_i\}_{i=1}^N \cap [0, \mathbf{x})}{N} - \mu([0, \mathbf{x}) \right|^p d\mathbf{x} \right)^{\frac{1}{p}}. \quad (6)$$

Clearly, the star-discrepancy D^* can be derived as a special case of (6) with $p = \infty$. Here, we focus on the case of $p = 2$ as our training objective, since instead of computing the integral in (6), we can leverage its closed-form expression, known as Warnock’s formula (Warnock, 1972),

$$\begin{aligned} \mathcal{L}_2^2(\{\mathbf{X}_i\}_{i=1}^N) &= \frac{1}{3^d} - \frac{2}{N} \sum_{i=0}^{N-1} \prod_{k=0}^d \frac{1 - \mathbf{X}_{i,k}^2}{2} \\ &+ \frac{1}{N^2} \sum_{i,j=0}^{N-1} \prod_{k=0}^d 1 - \max(\mathbf{X}_{i,k}, \mathbf{X}_{j,k}), \end{aligned} \quad (7)$$

where $\mathbf{X}_{i,k}$ is the k -th entry of \mathbf{X}_i . This enables a very fast and exact computation of the \mathcal{L}_2 -discrepancy without errors resulting from numerical quadrature methods. Thus, the \mathcal{L}_2 -discrepancy is an ideal candidate for the training objective of our machine learning approach.

3.4. Extension to higher dimensions

In many practical problems, particularly in engineering and finance, the dimension d of the problem can be very large. This necessitates extending low-discrepancy sequences to the high dimensional case of $d \gg 1$. However, it is known (Morokoff & Caffisch, 1994; Wang & Sloan, 2008) that the \mathcal{L}_2 -discrepancy fails to identify superior distributional properties of low-discrepancy point sets over random samples as the dimension increases. Indeed, in high dimensions the classical \mathcal{L}_2 -discrepancy of low-discrepancy point sets behaves like $\mathcal{O}(1/\sqrt{N})$, the same as for random points, for moderate values of N , while an improved order close to $\mathcal{O}(1/N)$ can only be seen for extremely large N . Empirical evidence for these last claims can be found in the discrepancy plots contained in (Morokoff & Caffisch, 1994).

To this end, we suggest to base our new training objective for higher-dimensional generation of low-discrepancy points

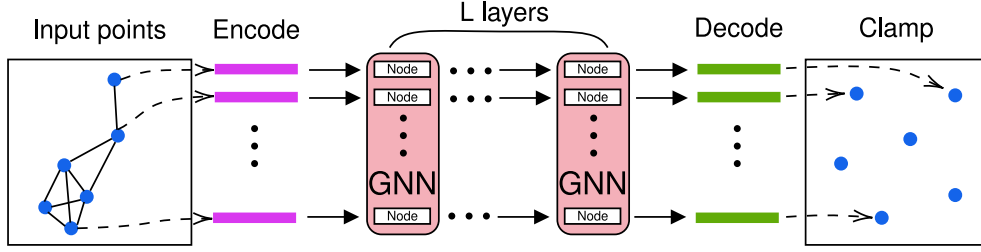


Figure 3. Schematic of the proposed model to learn low-discrepancy points. First, (random) input points $\{\mathbf{X}_i\}_{i=1}^N$ are encoded to a high dimensional representation. Second, the encoded representations are passed through a deep GNN (4), where the underlying computational graph is constructed based on nearest neighbors using the positions of the initial input points. Finally, the node-wise output representations of the final GNN layer are decoded and clamped yielding new d -dimensional points $\{\tilde{\mathbf{X}}_i\}_{i=1}^N$ in $[0, 1]^d$.

on the Hickernell \mathcal{L}_p -discrepancy (Hickernell, 1998),

$$D_{H,p}(\{\mathbf{X}_i\}_{i=1}^N) = \left(\sum_{\emptyset \neq s \subseteq \{1, \dots, d\}} \mathcal{L}_p^s(\{\mathbf{X}_i^s\}_{i=1}^N) \right)^{\frac{1}{p}}, \quad (8)$$

where $\emptyset \neq s \subseteq \{1, \dots, d\}$ is a non-empty subset of coordinate indices, and $\{\mathbf{X}_i^s\}_{i=1}^N$ is the projection of $\{\mathbf{X}_i\}_{i=1}^N$ onto $[0, 1]^{|s|}$. Note that while we can again make use of Warnock’s formula (7) to compute $D_{H,2}$, it requires computing the sum of the \mathcal{L}_2 -discrepancy of $2^d - 1$ projections, which already for $d = 32$ is more than 1B. This highlights the necessity of modifying $D_{H,2}$ in order for it to be used as a training objective in a machine learning framework. Therefore, we suggest to base the training objective on a modification of the Hickernell \mathcal{L}_p -discrepancy via random projections,

$$\tilde{D}_{H,p,K}(\{\mathbf{X}_i\}_{i=1}^N) = \left(\sum_{k=1}^K \mathcal{L}_p^{s_k}(\{\mathbf{X}_i^{s_k}\}_{i=1}^N) \right)^{\frac{1}{p}}, \quad (9)$$

where $\emptyset \neq s_k \sim \mathcal{P}(\{1, \dots, d\})$ are randomly sampled subsets of coordinate indices for each $k = 1, \dots, K$, thus requiring to compute the \mathcal{L}_p -discrepancy only K times.

Generating problem-dependent point sets. As a further advantage to this framework, we highlight its inherent flexibility. Specifically, employing the modified Hickernell discrepancy as the training objective represents a *first step towards an adaptive QMC sampling method tailored for specific problems*. It is widely recognized that for many problems, the effective dimension—essentially, the number of dimensions capturing the majority of the problem’s variability—is often significantly lower than the nominal dimension; for full details, refer to (Caffisch et al., 1997). Therefore, during high-dimensional training, prioritizing sampling from specific lower dimensional projections will yield a d -dimensional point set that is highly uniformly distributed in those same projections identified during training. This approach effectively creates a custom-made point set,

optimized for problems that primarily depend upon particular dimensions.

4. Empirical results

In this section, we present empirical results comparing MPMC points to current state-of-the-art low-discrepancy point sets. More concretely, we demonstrate superior distributional properties of MPMC over other low-discrepancy point sets mainly with respect to the star-discrepancy D^* .

As described above, computing the star-discrepancy is usually a difficult task. Being a discrete problem, depending on the number of points, a crude search for the worst distribution over all admissible test boxes is often extremely slow in low dimensions, and intractable even in dimension as small as four or five. The best known exact algorithm to calculate the star-discrepancy is the so-called Dopkin, Eppstein and Mitchell (DEM) algorithm (Dobkin et al., 1996) which runs in $\mathcal{O}(N^{1+d/2})$ time. In all experiments, the results of which are presented shortly, to calculate the star discrepancy we either use a simple crude search or a parallelized version of the DEM algorithm from (Clément et al., 2023) to speed up calculation when necessary. The interested reader is recommended to consult (Doerr et al., 2014) and references therein for more information on the calculation of the star-discrepancy, and indeed the computation of other discrepancy measures.

4.1. Low-dimensional generation of MPMC points

Here, we focus on generating MPMC points within a lower-dimensional setting particularly because this area has recently attracted significant attention (Clément et al., 2022; 2024; Clément et al., 2023) providing a solid basis for comparison. Additionally, QMC methods are known to perform very well on many complex applications as long as the low-dimensional projections of the underlying point set have low discrepancy. Therefore, generating 2- or 3-dimensional point sets with strong distributional properties are of paramount interest toward building competitive con-

structions performing well on a variety of problems.

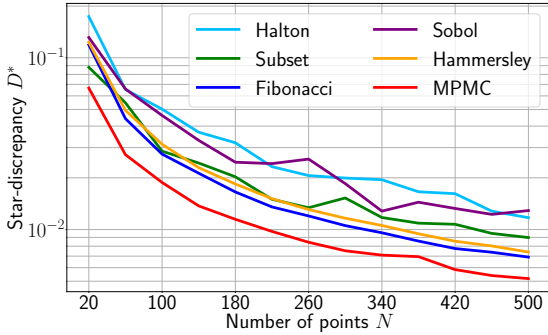


Figure 4. Star-discrepancy D^* of Halton, Sobol’, Subset Selection, Hammersley, Fibonacci, and MPMC for increasing number of points $N = 20, \dots, 500$ in $d = 2$.

We compare the irregularity of our MPMC point sets with a truncation to the first N points of the widely used Sobol’ and Halton sequences. We note that MPMC points are sets optimized for N chosen in advance, whereas a key advantage of the Sobol’ and Halton sequences are that they are built for repeated sampling and retain a low-discrepancy for all values of N . Therefore, in addition, we provide comparison with state-of-the-art point sets derived from the subset selection method from (Clément et al., 2022; 2024), the Hammersley construction in base $1 + \sqrt{2}$ as introduced in (Kirk et al., 2023) and the Fibonacci set defined as $\{(i/n, \{i\varphi\}) : i \in \{0, \dots, n - 1\}\}$ where φ represents the golden ratio, the notation $\{x\}$ denotes the fractional part of $x \in \mathbb{R}$. All three of these sets are recognized for having among the lowest star-discrepancy for given N in two dimensions. Fig. 4 shows the star-discrepancy of MPMC, Sobol’, Halton, subset selection, Hammersley and Fibonacci sets in two dimensions for increasing number of points $N = 20, \dots, 500$. We can see that MPMC significantly outperforms all other methods with respect to the star-discrepancy. In fact, the star-discrepancy of MPMC is on average 1.5 times smaller than that of the current state-of-the-art Fibonacci construction, and on average more than 2.5 times smaller than Sobol’ or Halton points. We provide the exact values of Fig. 4 in the Supporting Information (SI) such that it can serve as a benchmark for future methods.

4.2. Optimality of MPMC point sets

Much of the past research on low-discrepancy point sets focused on achieving star-discrepancy with optimal asymptotic order in N for implementation in quasi-Monte Carlo methods. However, there has been a recent surge in interest in finding point sets that minimize discrepancy for fixed N and d . The main contribution in this direction was given in

(Clément et al., 2023), where the authors constructed optimal star-discrepancy point sets in two and three dimensions. Naturally, we are interested in comparing MPMC points to these optimal formulations. The results of the optimal star-discrepancy comparison in two dimensions are presented in Table 1 and the three dimensional case is found in the SI.

Table 1. Comparison in two dimensions of MPMC star-discrepancy values against optimal sets and Fibonacci sets.

N	1	2	3	4	5
Fibonacci	1.0	0.6909	0.5880	0.4910	0.3528
Optimal	$1/\varphi$	0.366	0.2847	0.25	0.2
MPMC	$1/\varphi$	0.366	0.2847	0.25	0.2

N	6	7	8	9	10
Fibonacci	0.3183	0.2728	0.2553	0.2270	0.2042
Optimal	0.1667	0.15	0.1328	0.1235	0.1111
MPMC	0.1692	0.1508	0.1354	0.1240	0.1124

N	11	12	13	14	15
Fibonacci	0.1857	0.1702	0.1571	0.1459	0.1390
Optimal	0.1030	0.0952	0.0889	0.0837	0.0782
MPMC	0.1058	0.0975	0.0908	0.0853	0.0794

N	16	17	18	19	20
Fibonacci	0.1486	0.1398	0.1320	0.1251	0.1188
Optimal	0.0739	0.0699	0.0666	0.0634	0.0604
MPMC	0.0768	0.0731	0.0699	0.0668	0.0640

We can see that the star-discrepancy of MPMC points is very close to the star-discrepancy of the optimal point sets, and in fact match it exactly for small N . Moreover, the star-discrepancy of the Fibonacci set is far off the optimal values, i.e., approximately by a factor of 2. Finally, it is worth highlighting that the computation of the optimal points requires to solve a non-linear programming problem and takes approximately 18 days to compute. In contrast to that, our model generating MPMC points can be trained from scratch in less than 5 minutes on a conventional GPU machine.

4.3. MPMC generation in high dimensions

As discussed in Section 3.4, the efficacy of discrepancy measures to justly evaluate irregularity of distribution is flawed in higher dimensions. Therefore, to alternatively assess the quality of the distribution of higher dimensional point sets and sequences, motivated by the Koksma-Hlawka inequality (2), we will implement high dimensional MPMC points in an integral arising in a real-world problem from computational finance previously studied in (Lemieux & Owen, 2002; Wang & Sloan, 2005; Faure & Lemieux, 2009).

The primary goal is to accurately estimate the value at time 0 of an Asian call option on an underlying asset that follows a log-normal distribution. Complete details of the problem

formulation are provided in the SI. Table 2 shows the absolute errors observed when implementing Halton, Sobol’ and MPMC constructions. With our chosen parameters, this problem is known (Lemieux & Owen, 2002) to exhibit more than 97% of its variability in dimensions one, two, and three. Therefore, we train a 32-dimensional MPMC point set while emphasizing the 1-3-dimensional projections as described in Section 3.4. We report the average absolute error of an MPMC training batch, which is selected based on the minimal Hickernell \mathcal{L}_2 -discrepancy restricted to 1-3-dimensional projections.

Table 2. Approximation error of an Asian call option pricing of MPMC, Halton and Sobol’.

N	32	64	128	256	512
Halton	6.4566	4.1580	3.5590	2.8046	1.9376
Sobol	1.2163	1.3545	0.9470	0.6043	0.4784
MPMC	1.3836	0.8129	0.4937	0.2317	0.1019

Once again, the 32-dimensional MPMC point sets show significant enhancements over Halton and Sobol’. This improvement is particularly notable at higher values of N , where MPMC outperforms Sobol’ by a factor of approximately 5, and Halton by a factor of approximately 19. The efficiency observed in this high-dimensional problem is promising and suggests a superior uniformity of MPMC points. In fact, the observed improvements may partially be explained by the uniformity held in lower-dimensional projections when compared to the traditional choices of QMC point sets. We refer to the SI for further discussion.

4.4. Ablations

Our proposed MPMC method is the result of several design choices, such as the type of input points, the deep learning model, and the training objective. In order to further justify our choices, we ablate several aspects of our MPMC framework illustrated by the following questions:

How does the graph structure influence the performance? To answer this, we compute the average \mathcal{L}_2 -discrepancy of several trained MPMC models for increasing values of the nearest neighbor radius r in (5) ranging from 0 to 1 for different number of points $N = 64, 128, 1024$, and plot the results in the SI. These results lead to two important observations. First, not using a graph structure at all, i.e., setting $r = 0$ resulting in Deepsets (Zaheer et al., 2017), significantly impairs the performance of MPMC, reaching average \mathcal{L}_2 -discrepancy values that are 9 to 40 times worse than using a graph structure. The second observation is that although the performance of MPMC is relatively stable for any choice of $r > 0$, including the radius r in hyperparameter tuning can help achieve point sets with minimal discrepancy.

What is the role of the GNN architecture used in MPMC? While we base MPMC on message-passing neural networks (MPNNs) (Gilmer et al., 2017), other GNN architectures such as Graph Convolutional Networks (GCNs) (Kipf & Welling, 2017), or Graph Attention Networks (GATs) can be used in this context as well. To check this, we train MPMC based on MPNNs, GCNs, and GATs for three different number of points $N = 64, 256, 1024$ and show the \mathcal{L}_2 -discrepancy in the SI. Based on these results, we conclude that GCNs and GATs outperform each other based on the number of points N . At the same time, MPNNs consistently yield point sets with the lowest discrepancy values among all three considered GNN architectures.

Does the choice of input point sets described in Section 3.1 influence the performance of MPMC? To answer this, we train several MPMC models on all three different types of input points, i.e., random points, Sobol’, and a randomized Sobol’, where we choose $\xi \sim \mathcal{U}([0, 0.1]^d)$ in (3), for two different number of points $N = 256, 1024$. We report the average \mathcal{L}_2 -discrepancy of all trained MPMC models for increasing number of training steps in the SI. We observe that on average Sobol’ and randomized Sobol’ yield slightly lower discrepancy values and faster convergence compared to random points and thus lead to a more robust performance. However, we further note, that instead of averaging over all trained MPMC models, but instead choosing the single best model yield similar results for each input point type.

5. Discussion

Low-discrepancy points play a central role in many applications in science and engineering. In this article, we have proposed MPMC, the first machine learning approach to generate new sets of low-discrepancy points. Inspired by the geometric nature of constructing such point sets, we base our MPMC approach on GNNs. Choosing an adequate training objective, i.e., closed-form solution of the \mathcal{L}_2 -discrepancy, we show that MPMC successfully transforms (random) input points into point sets with low discrepancy. Moreover, we extend this framework to higher dimensions, by training with an approximation of the Hickernell \mathcal{L}_2 -discrepancy. We further present an extensive empirical evaluation to illustrate different aspects of the proposed MPMC approach, highlighting the superior distributional properties of MPMC points compared to previous state-of-the-art methods. Finally, we carefully ablate key components of our MPMC model, yielding deeper empirical insights.

MPMC represents a novel and efficient way of generating point sets with very low discrepancy. In fact, MPMC is shown to obtain optimal or near-optimal discrepancy in near-real time. This is crucial for computationally expensive applications, where MPMC will lead to potentially significantly lower absolute errors compared to previous methods.

Moreover, the generality of the MPMC framework allows for designing tailor-made QMC points that exploit specific structures of the problem at hand.

The aim of this paper was to generate point sets with low discrepancy for a fixed dimension and fixed number of points. On the other hand, many important applications require repeated sampling resulting in low-discrepancy sequences and not fixed point sets. Thus, one important aspect of future work will be to extend our MPMC point sets to MPMC sequences. Another essential part of this paper was on studying the distributional properties of MPMC points, in contrast to simply showcasing their performance in practical applications. However, based on the empirical evidence in this paper, we expect MPMC point sets to excel in various applications. Motivated by this, we would like to apply MPMC to various problems in science and engineering as future work.

References

Branicky, M. S., LaValle, S. M., Olson, K., and Yang, L. Quasi-randomized path planning. In *Proceedings 2001 ICRA. IEEE International Conference on Robotics and Automation (Cat. No. 01CH37164)*, volume 2, pp. 1481–1487. IEEE, 2001.

Bronstein, M. M., Bruna, J., Cohen, T., and Veličković, P. Geometric deep learning: Grids, groups, graphs, geodesics, and gauges. *arXiv:2104.13478*, 2021.

Bruna, J., Zaremba, W., Szlam, A., and LeCun, Y. Spectral networks and locally connected networks on graphs. In *2nd International Conference on Learning Representations, ICLR 2014*, 2014.

Caffisch, R. E., Morokoff, W. J., and Owen, A. B. Valuation of mortgage-backed securities using brownian bridges to reduce effective dimension. *Journal of Computational Finance*, 1:27–46, 1997.

Cauwet, M.-L., Couprie, C., Dehos, J., Luc, P., Rapin, J., Riviere, M., Teytaud, F., Teytaud, O., and Usunier, N. Fully parallel hyperparameter search: Reshaped space-filling. In *International Conference on Machine Learning*, pp. 1338–1348. PMLR, 2020.

Clément, F., Doerr, C., and Paquete, L. Star discrepancy subset selection: problem formulation and efficient approaches for low dimensions. *J. Complexity*, 70:Paper No. 101645, 34, 2022. ISSN 0885-064X,1090-2708.

Clément, F., Vermetten, D., De Nobel, J., Jesus, A. D., Paquete, L., and Doerr, C. Computing star discrepancies with numerical black-box optimization algorithms. In *Proceedings of the Genetic and Evolutionary Computation Conference, GECCO '23*, pp. 1330–1338, New York,

NY, USA, 2023. Association for Computing Machinery. ISBN 9798400701191.

Clément, F., Doerr, C., and Paquete, L. Heuristic approaches to obtain low-discrepancy point sets via subset selection. *J. Complexity*, 83:Paper No. 101852, 2024. ISSN 0885-064X,1090-2708.

Clément, F., Doerr, C., Klamroth, K., and Paquete, L. Constructing optimal \mathcal{L}_∞ star discrepancy sets. *Preprint*, 2023. <https://arxiv.org/abs/2311.17463>.

Defferrard, M., Bresson, X., and Vandergheynst, P. Convolutional neural networks on graphs with fast localized spectral filtering. *Advances in neural information processing systems*, 29:3844–3852, 2016.

Derrow-Pinion, A., She, J., Wong, D., Lange, O., Hester, T., Perez, L., Nunkesser, M., Lee, S., Guo, X., Battaglia, P. W., Gupta, V., Li, A., Xu, Z., Sanchez-Gonzalez, A., Li, Y., and Veličković, P. Eta prediction with graph neural networks in google maps. In *Proceedings of the 30th ACM International Conference on Information & Knowledge Management*, pp. 3767–3776, 2021.

Dick, J., Kritzer, P., and Pillichshammer, F. *Constructions of Lattice Rules*, pp. 95–139. Springer International Publishing, Cham, 2022.

Dobkin, D. P., Eppstein, D., and Mitchell, D. P. Computing the discrepancy with applications to supersampling patterns. *ACM Trans. Graph.*, 15(4):354–376, oct 1996. ISSN 0730-0301.

Doerr, B., Gnewuch, M., and Srivastav, A. Bounds and constructions for the star-discrepancy via δ -covers. *J. Complexity*, 21(5):691–709, 2005. ISSN 0885-064X,1090-2708. doi: 10.1016/j.jco.2005.05.002. URL <https://doi.org/10.1016/j.jco.2005.05.002>.

Doerr, C. and De Rainville, F.-M. Constructing low star discrepancy point sets with genetic algorithms. In *Proceedings of the 15th Annual Conference on Genetic and Evolutionary Computation*, pp. 789–796, New York, NY, USA, 2013. Association for Computing Machinery. ISBN 9781450319638.

Doerr, C., Gnewuch, M., and Wahlström, M. *Calculation of Discrepancy Measures and Applications*, pp. 621–678. Springer International Publishing, 2014.

Drmotá, M. and Tichy, R. F. *Sequences, discrepancies and applications*, volume 1651 of *Lecture Notes in Mathematics*. Springer-Verlag, Berlin, 1997. ISBN 3-540-62606-9. doi: 10.1007/BFb0093404. URL <https://doi.org/10.1007/BFb0093404>.

- 440 Faure, H. Discrepance de suites associées à un système
441 de numération (en dimension s). *Acta Arithmetica*, 41:
442 337–351, 1982.
- 443 Faure, H. and Lemieux, C. Generalized halton sequences in
444 2008: A comparative study. *ACM Trans. Model. Comput.*
445 *Simul.*, 19(4), 2009. ISSN 1049-3301.
- 446 Frasconi, P., Gori, M., and Sperduti, A. A general frame-
447 work for adaptive processing of data structures. *IEEE*
448 *Trans. Neural Networks*, 9(5):768–786, 1998.
- 449 Galanti, S. and Jung, A. Low-discrepancy sequences: Monte
450 carlo simulation of option prices. *J. Deriv.*, pp. 63–83,
451 1997.
- 452 Gaudalet, T., Day, B., Jamasb, A. R., Soman, J., Regep,
453 C., Liu, G., Hayter, J. B., Vickers, R., Roberts, C., Tang,
454 J., et al. Utilizing graph machine learning within drug
455 discovery and development. *Briefings in Bioinformatics*,
456 22(6), 2021.
- 457 Giannopoulos, P., Knauer, C., Wahlström, M., and Werner,
458 D. Hardness of discrepancy computation and ϵ -net
459 verification in high dimension. *J. Complexity*, 28(2):
460 162–176, 2012. ISSN 0885-064X,1090-2708. doi:
461 10.1016/j.jco.2011.09.001. URL [https://doi.org/](https://doi.org/10.1016/j.jco.2011.09.001)
462 [10.1016/j.jco.2011.09.001](https://doi.org/10.1016/j.jco.2011.09.001).
- 463 Gilmer, J., Schoenholz, S. S., Riley, P. F., Vinyals, O., and
464 Dahl, G. E. Neural message passing for quantum chem-
465 istry. In *ICML*, 2017.
- 466 Glasserman, P. *Monte Carlo methods in financial engi-*
467 *neering*. Springer, New York, 2004. ISBN 0387004513
468 9780387004518 1441918221 9781441918222.
- 469 Gnewuch, M., Srivastav, A., and Winzen, C. Finding op-
470 timal volume subintervals with k -points and calculating
471 the star discrepancy are NP-hard problems. *J. Complexity*,
472 25(2):115–127, 2009. ISSN 0885-064X,1090-2708.
- 473 Goller, C. and Kuchler, A. Learning task-dependent
474 distributed representations by backpropagation through
475 structure. In *ICNN*, 1996.
- 476 Gori, M., Monfardini, G., and Scarselli, F. A new model for
477 learning in graph domains. In *IJCNN*, 2005.
- 478 Haber, S. Numerical evaluation of multiple integrals. *SIAM*
479 *Review*, (12):481–526, 1970.
- 480 Halton, J. H. On the efficiency of certain quasi-random
481 sequences of points in evaluating multi-dimensional inte-
482 grals. *Numer. Math.*, 2:84–90, 1960.
- 483 Hickernell, F. A generalized discrepancy and quadrature
484 error bound. *Mathematics of computation*, 67(221):299–
485 322, 1998.
- 486 Hlawka, E. *The theory of uniform distribution*. A B Aca-
487 demic Publishers, Berkhamsted, 1984. ISBN 0-907360-
488 02-5.
- 489 Kipf, T. N. and Welling, M. Semi-supervised classification
490 with graph convolutional networks. In *ICLR*, 2017.
- 491 Kirk, N., Lemieux, C., and Wiart, J. Golden ratio nets and se-
492 quences. *Preprint*, 2023. <http://arxiv.org/abs/2312.11696>.
- 493 Korobov, N. Number-theoretic methods of approximate
494 analysis. *Fizmatgiz, Moscow*, 1963. In Russian.
- 495 Kuipers, L. and Niederreiter, H. *Uniform distribution*
496 *of sequences*. Pure and Applied Mathematics. Wiley-
497 Interscience [John Wiley & Sons], New York-London-
498 Sydney, 1974.
- 499 Lemieux, C. *Monte Carlo and quasi-Monte Carlo sampling*.
500 Springer Series in Statistics. Springer, New York, 2009.
501 ISBN 978-0-387-78164-8.
- 502 Lemieux, C. and Owen, A. B. Quasi-regression and the
503 relative importance of the anova components of a function.
504 In Fang, K.-T., Niederreiter, H., and Hickernell, F. J.
505 (eds.), *Monte Carlo and Quasi-Monte Carlo Methods*
506 *2000*, pp. 331–344, Berlin, Heidelberg, 2002. Springer
507 Berlin Heidelberg.
- 508 Longo, M., Mishra, S., Rusch, T. K., and Schwab, C. Higher-
509 order quasi-monte carlo training of deep neural networks.
510 *SIAM Journal on Scientific Computing*, 43(6):A3938–
511 A3966, 2021.
- 512 L’Ecuyer, P. Quasi-monte carlo methods with applications
513 in finance. *Finance and Stochastics*, 13:307–349, 2009.
- 514 Mildenhall, B., Srinivasan, P. P., Tancik, M., Barron, J. T.,
515 Ramamoorthi, R., and Ng, R. Nerf: Representing scenes
516 as neural radiance fields for view synthesis. *Communica-*
517 *tions of the ACM*, 65(1):99–106, 2021.
- 518 Mishra, S. and Rusch, T. K. Enhancing accuracy of deep
519 learning algorithms by training with low-discrepancy se-
520 quences. *SIAM Journal on Numerical Analysis*, 59(3):
521 1811–1834, 2021.
- 522 Monti, F., Boscaini, D., Masci, J., Rodola, E., Svoboda, J.,
523 and Bronstein, M. M. Geometric deep learning on graphs
524 and manifolds using mixture model cnns. In *CVPR*, 2017.
- 525 Morokoff, W. J. and Caflisch, R. E. Quasi-random se-
526 quences and their discrepancies. *SIAM Journal on Sci-*
527 *entific Computing*, 15(6):1251–1279, 1994. doi: <https://doi.org/10.1137/0915077>.
- 528 Niederreiter, H. Discrepancy and convex programming.
529 *Annali di Matematica*, 93:89–97, 1972.

- 495 Niederreiter, H. Point sets and sequences with small dis-
 496 crepancy. *Monatshefte für Mathematik*, 104(4):273–337,
 497 1987.
- 498 Niederreiter, H. *Random Number Generation and Quasi-
 499 Monte Carlo Methods*. 1992.
- 501 Novak, E. and Woźniakowski, H. *Tractability of multi-
 502 variate problems. Volume II: Standard information for
 503 functionals*, volume 12 of *EMS Tracts in Mathematics*.
 504 European Mathematical Society (EMS), Zürich, 2010.
 505 ISBN 978-3-03719-084-5.
- 506 Nuyens, D. *The construction of good lattice rules and
 507 polynomial lattice rules*, pp. 223–256. De Gruyter, Berlin,
 508 Boston, 2014.
- 510 Paulin, L., Bonneel, N., Coeurjolly, D., Iehl, J.-C., Keller,
 511 A., and Ostromoukhov, V. Matbuilder: Mastering sam-
 512 pling uniformity over projections. *ACM Transactions on
 513 Graphics (TOG)*, 41(4):1–13, 2022.
- 515 Roth, K. F. On irregularities of distribution. *Mathematika*,
 516 1:73–79, 1954. ISSN 0025-5793.
- 517 Scarselli, F., Gori, M., Tsoi, A. C., Hagenbuchner, M., and
 518 Monfardini, G. The graph neural network model. *IEEE
 519 Trans. Neural Networks*, 20(1):61–80, 2008.
- 521 Shlomi, J., Battaglia, P., and Vlimant, J.-R. Graph neural
 522 networks in particle physics. *Machine Learning: Science
 523 and Technology*, 2(2):021001, 2020.
- 524 Sloan, I. H. and Joe, S. *Lattice Methods for Multiple
 525 Integration*. Oxford University Press, 1994. ISBN
 526 9780198534723.
- 528 Sobol’, I. On the distribution of points in a cube and the ap-
 529 proximate evaluation of integrals. *USSR Computational
 530 Mathematics and Mathematical Physics*, 7(4):86–112,
 531 1967. ISSN 0041-5553.
- 533 Sperduti, A. Encoding labeled graphs by labeling RAAM.
 534 In *NIPS*, 1994.
- 535 Sperduti, A. and Starita, A. Supervised neural networks
 536 for the classification of structures. *IEEE Trans. Neural
 537 Networks*, 8(3):714–735, 1997.
- 539 van der Corput, J. Verteilungsfunktionen i–ii. *Proc. Akad.
 540 Amsterdam*, 38:813–821, 1058–1066, 1935.
- 541 Velickovic, P., Cucurull, G., Casanova, A., Romero, A.,
 542 Liò, P., and Bengio, Y. Graph attention networks. In *6th
 543 International Conference on Learning Representations,
 544 ICLR*, 2018.
- 546 Wang, X. and Sloan, I. H. Why are high-dimensional fi-
 547 nance problems often of low effective dimension? *SIAM
 548 Journal on Scientific Computing*, 27(1):159–183, 2005.
- 549 Wang, X. and Sloan, I. H. Low discrepancy sequences
 in high dimensions: How well are their projections dis-
 tributed? *Journal of Computational and Applied Math-
 ematics*, 213(2):366–386, 2008. ISSN 0377-0427. doi:
<https://doi.org/10.1016/j.cam.2007.01.005>.
- Warnock, T. T. Computational investigations of low-
 discrepancy point sets. In *Applications of number theory
 to numerical analysis*, pp. 319–343. Elsevier, 1972.
- Ying, R., He, R., Chen, K., Eksombatchai, P., Hamilton,
 W. L., and Leskovec, J. Graph convolutional neural net-
 works for web-scale recommender systems. In *KDD*,
 2018.
- Zaheer, M., Kottur, S., Ravanbakhsh, S., Poczos, B.,
 Salakhutdinov, R. R., and Smola, A. J. Deep sets. *Ad-
 vances in neural information processing systems*, 30,
 2017.
- Zhou, J., Cui, G., Zhang, Z., Yang, C., Liu, Z., Wang, L., ,
 Li, C., and Sun, M. Graph neural networks: a review of
 methods and applications. *arXiv:1812.08434v4*, 2019.

Supplementary Material for:

Message-Passing Monte Carlo: Generating low-discrepancy point sets via Graph Neural Networks

A. Training details

All experiments have been run on NVIDIA GeForce RTX 2080 Ti, GeForce RTX 3090, TITAN RTX and Quadro RTX 6000 GPUs. Each model was trained for initial 100k training steps, after which the learning rate was reduced by a factor of 10 whenever the discrepancy measure of the output point sets did not improve for a total of 2k training steps evaluated after every 100 training steps. The training was stopped once the learning rate reached a value less than 10^{-6} . Moreover, the hyperparameters of the model were tuned based on random search according to Table 3, which shows the search-space of each hyperparameter as well as the random distribution used to sample from it.

Table 3. Hyperparameter search-space and random distributions to sample from it.

	range	distribution
learning rate	$[10^{-4}, 10^{-2}]$	log uniform
hidden size $m_0 = m_1 = \dots = m_L$	$\{32, 64, 128, 256\}$	disc. uniform
number of GNN layers L	$\{1, 2, \dots, 10\}$	disc. uniform
size of mini-batches	$\{8, 16, 32\}$	disc. uniform
weight decay	$[10^{-8}, 10^{-2}]$	log uniform

B. The Asian Option Problem Formulation

We describe the problem of estimating the value at time 0 of an Asian call option on an underlying asset in detail. The results of which are presented in the main text as Table 2.

The main goal is to estimate an expectation of the form,

$$C_0 = \mathbb{E} \left[e^{-rT} \left(\frac{1}{d} \sum_{j=1}^d S(u_j) - K \right)^+ \right].$$

We let T be the expiration time of the contract, K the strike price, for $Z \sim N(0, 1)$ let $S(u) = S(0)e^{(r-\frac{\sigma^2}{2})u+\sigma\sqrt{u}Z}$ be the price of the underlying asset at time u , and $0 < u_1 < \dots < u_d = T$ are d times at which the asset price is observed in order to compute the average used in the option pricing formula. The expectation is taken under the risk-neutral probability measure. Finally, r is the risk-free rate, the notation x^+ means $\max(0, x)$, Φ^{-1} is the inverse CDF of the standard normal distribution and $\Delta_l = u_l - u_{l-1}$. Assuming the stock price follows a geometric Brownian motion with volatility σ , it can be shown that this expectation can be written as follows:

$$C_0 = e^{-rT} \int_{[0,1]^d} \left(\frac{1}{d} \sum_{j=1}^d S(0)e^{(r-\frac{\sigma^2}{2})u_j+\sigma\sum_{i=1}^j\sqrt{\Delta_i}\Phi^{-1}(x_i)} - K \right)^+ dx_1 \dots dx_d.$$

In our simulations, the true value $C_0 = 7.04704$ was calculated in advance via QMC simulation with 2M Sobol’ points with the following set of parameters: $S(0) = 50, T = 1$ year, $r = 0.05, \sigma = 0.3, K = 45$ and $d = 32$.

C. Further empirical insights

C.1. Structure of MPMC Points

Initially explored in (Clément et al., 2023), the authors provide insights into the configurations of two dimensional point sets that achieve optimal star-discrepancy by providing visualizations of the local discrepancy within the unit square. Providing equivalent comparisons, Figure 5 displays the local discrepancy plots for Sobol’ sequences, MPMC points, and optimal point sets, respectively. Each plot has its own color scale where darker areas indicate lower local discrepancy values, and

brighter areas denote higher values. The presence of a black dot in each plot marks the point of maximum local discrepancy, i.e., the explicit anchored test box where the star-discrepancy is obtained. Additionally, regions of high local discrepancy form bright triangular regions whose corner is either directed toward the upper right corner to represent open boxes with too few points, or angled toward the lower left, indicating closed boxes with an excess of points. For instance, the Sobol' plots exclusively show closed overfilled boxes, with bright triangles pointing downward and leftward toward the origin.

A visual comparison reveals structural similarities between the optimal sets and the MPMC points, suggesting a more balanced distribution of local discrepancy values across the unit square, with both open and closed boxes appearing in the plots. Interestingly, this similar structure emerges despite the sets consisting of quite different exact point values.

In conclusion, it seems evident that the GNN captures an essential underlying local discrepancy structure, which is key for minimizing star-discrepancy.

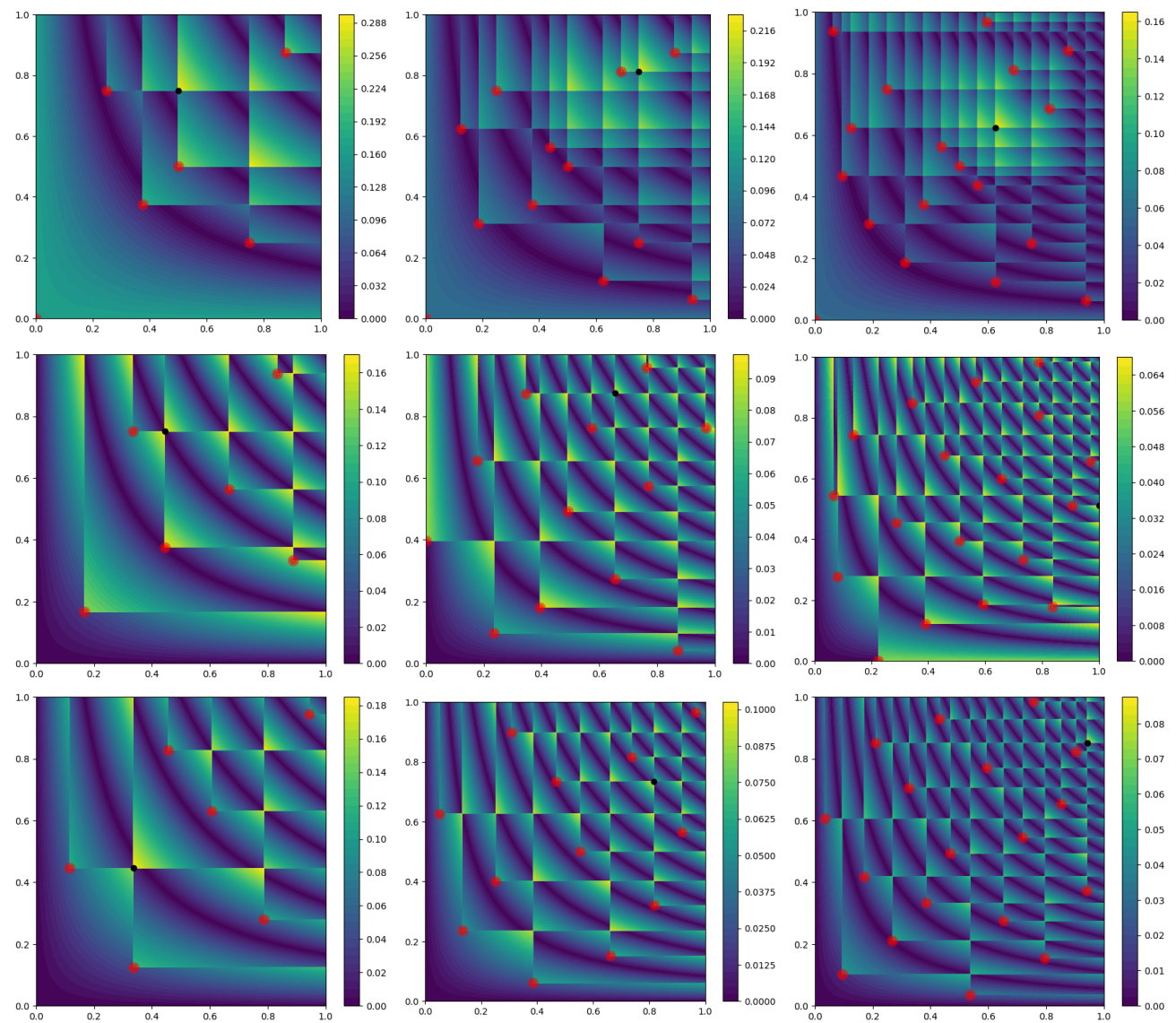


Figure 5. Local discrepancy plots for Sobol' sequence (top), optimal point sets obtained in (Clément et al., 2023) (middle row), and MPMC point sets (bottom) for $N = 6$ points (left), $N = 12$ points (middle column), and $N = 18$ points (right).

C.2. Projections of MPMC points

As noted in the main text, when applied to the computational finance integral described in Section B to estimate the value of an Asian call option, the MPMC points far outperform the Sobol' or Halton in terms of approximation accuracy. A significantly important factor for the success of QMC methods in high dimensional application is the quality of the distribution in the lower dimensional projections of the QMC point set. See (Lemieux & Owen, 2002) for a more comprehensive discussion. Figure 6 and 7 display the 5-th and 6-th, and 26-th and 27-th coordinate projections respectively of the MPMC points, Sobol' and Halton sequences constructed in 32 dimensions. Visual inspection reveals that the projections seem to be just as uniformly distributed in the 5-th and 6-th dimensions and notably more evenly distributed as the dimension increases to 26 and 27. At these higher dimensions, we start noticing some undesired correlations in the coordinates of the Sobol' and Halton sequences, however, fortunately the MPMC construction does not exhibit this problematic feature displaying no significant correlation, clustering, or sparsity; the MPMC point sets appear random yet maintain a high degree of uniformity. This characteristic is particularly advantageous for tackling high-dimensional problems.

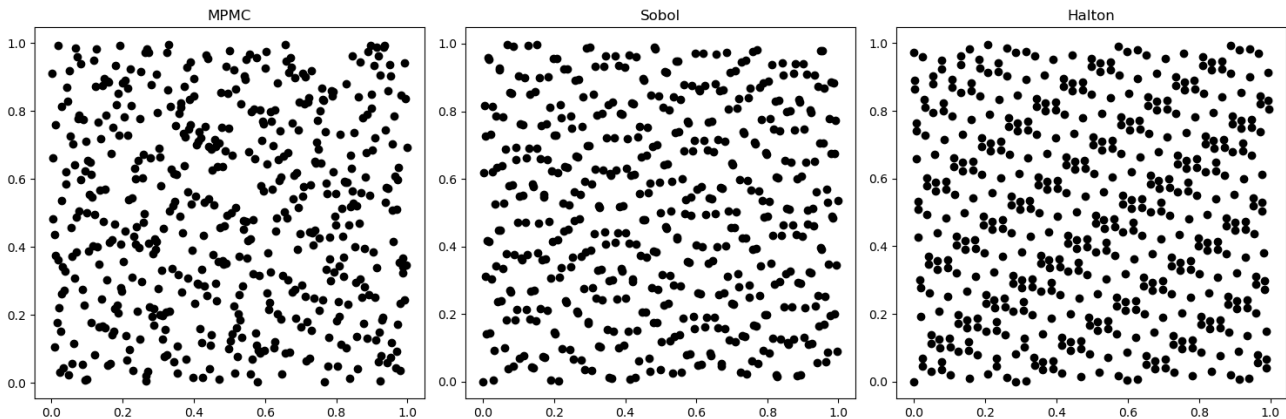


Figure 6. Projections of the 5-th and 6-th coordinates of 32-dimensional MPMC (left), Sobol' (middle) and Halton (right) with $N = 512$.

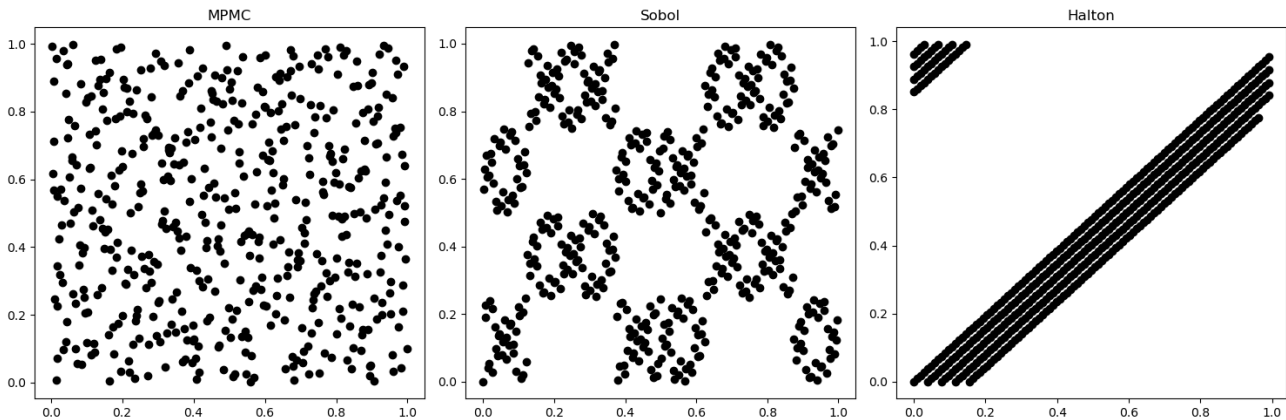


Figure 7. Projections of the 26-th and 27-th coordinates of 32-dimensional MPMC (left), Sobol' (middle) and Halton (right) with $N = 512$.

C.3. Optimality of MPMC in Three Dimensions

Table 4 shows the star-discrepancy of MPMC in three dimensions for $N = 1, 2, \dots, 8$ number of points, as well as the optimal star-discrepancy values obtained from (Clément et al., 2023). We can see that MPMC obtains again near-optimal star-discrepancy for all choices of N .

Table 4. Comparison in three dimensions of MPMC points star-discrepancy values against optimal sets.

N	1	2	3	4	5	6	7	8
Optimal	0.6823	0.4239	0.3445	0.3038	0.2618	0.2326	0.2090	0.1875
MPMC	0.6833	0.4239	0.3491	0.3071	0.2669	0.2371	0.2158	0.1993

C.4. Star-discrepancy values of Figure 4 in the main text

From the main text, we present the exact numerical values of the star-discrepancy for Halton, Sobol’, Subset Selection, Hammersley, Fibonacci, and MPMC points as a benchmark for future methods.

Table 5. Star-discrepancy values of Figure 4 in the main text for Halton, Sobol’, Subset Selection, Hammersley, Fibonacci, and MPMC.

N	20	60	100	140	180	220	260	300	340	380	420	460	500
Halton	0.1738	0.0654	0.0502	0.0369	0.032	0.0232	0.0206	0.0199	0.0195	0.0166	0.0162	0.0128	0.0117
Sobol	0.1312	0.0658	0.0462	0.0331	0.0247	0.0242	0.0257	0.0185	0.0128	0.0144	0.0133	0.0123	0.0129
Subset Selection	0.0880	0.0547	0.0286	0.0244	0.0203	0.015	0.0134	0.0153	0.0117	0.0109	0.0107	0.0095	0.0090
Hammersley	0.1230	0.0494	0.0314	0.0229	0.0184	0.0151	0.0131	0.0116	0.0106	0.0094	0.0085	0.008	0.0074
Fibonacci	0.1188	0.0442	0.0275	0.0213	0.0165	0.0135	0.012	0.0105	0.0096	0.0086	0.0078	0.0071	0.0065
MPMC	0.0666	0.0273	0.0188	0.0137	0.0115	0.0097	0.0084	0.0075	0.0071	0.0070	0.0058	0.0054	0.0052

C.5. On the role of the radius in the nearest neighbor graph

We recall from the main text, that our proposed MPMC method is based on GNNs that leverage r -radius nearest neighbors as the underlying computational graph, connecting nodes within a given radius r . How does the performance of MPMC depend on the radius r ? Moreover, is it necessary to use GNNs? To answer this, we train 10 MPMC models for different radius values $r = 0.1, \dots, 1.0$ for different number of points N and plot the resulting average \mathcal{L}_2 -discrepancy in Fig. 8. We can see that there is no correlation between the performance and a fixed radius r . Moreover, the performance appears to be not overly sensitive with respect to different values for the radius. Nevertheless, small variations of the performance with respect to the radius r can be seen and it is thus advisable to include the radius to the set of tune-able hyperparameters of the model.

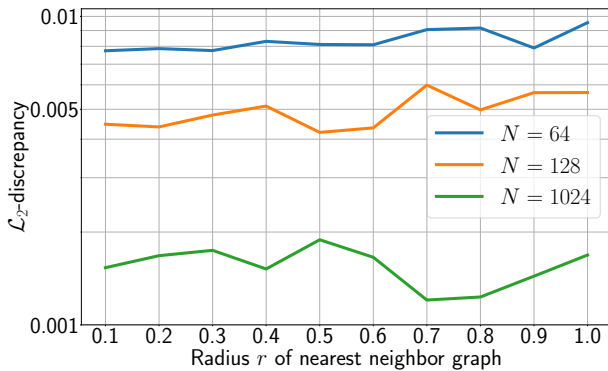


Figure 8. \mathcal{L}_2 -discrepancy of MPMC points for increasing values of the radius of the underlying nearest neighbor computational graph ranging from 0.1 to 1.0 for different number of points $N = 64, 128, 1024$.

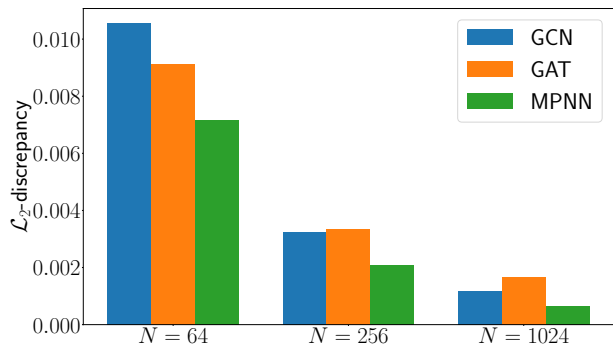


Figure 9. \mathcal{L}_2 -discrepancy of MPMC for different choices of GNN architectures, i.e., GCN (Kipf & Welling, 2017), GAT (Velickovic et al., 2018), and MPNN (Gilmer et al., 2017) for three different number of points $N = 64, 256, 1024$.

We further note that a radius of $r = 0$ corresponds to zero edges in the underlying computational graph. Thus, the model becomes a deepset (Zaheer et al., 2017), processing each point in the set individually without aggregating any neighborhood

information. The average \mathcal{L}_2 -discrepancy of this deepset is approximately 0.073 for $N = 64$, 0.058 for $N = 128$, and 0.063 for $N = 1024$, i.e., between 9 to over 40 times worse than GNNs with $r \geq 0.1$. Moreover, the deepset fails to decrease the \mathcal{L}_2 -discrepancy for increasing number of points N . This highlights the necessity of using GNNs that aggregate geometric information from neighboring points for successfully generating low-discrepancy point sets.

C.6. On the role of the GNN architecture

While we base our proposed MPMC model on MPNNs (Gilmer et al., 2017), any other GNN architecture could be used instead. Therefore, it is natural to ask how the choice of the GNN architecture influences the performance of MPMC. To answer this, we test three different configurations of MPMC: one based on MPNNs, one based on GCNs (Kipf & Welling, 2017), and one based on GATs (Velickovic et al., 2018). We train all three configurations for different number of points $N = 64, 256, 1024$, and provide the results as a bar plot in Fig. 9. We can see that while GCNs and GATs outperform each other depending on the chosen number of points, MPNNs consistently produce point sets with the lowest \mathcal{L}_2 -discrepancy among all three configurations for all number of points considered here.

C.7. On the role of the input points

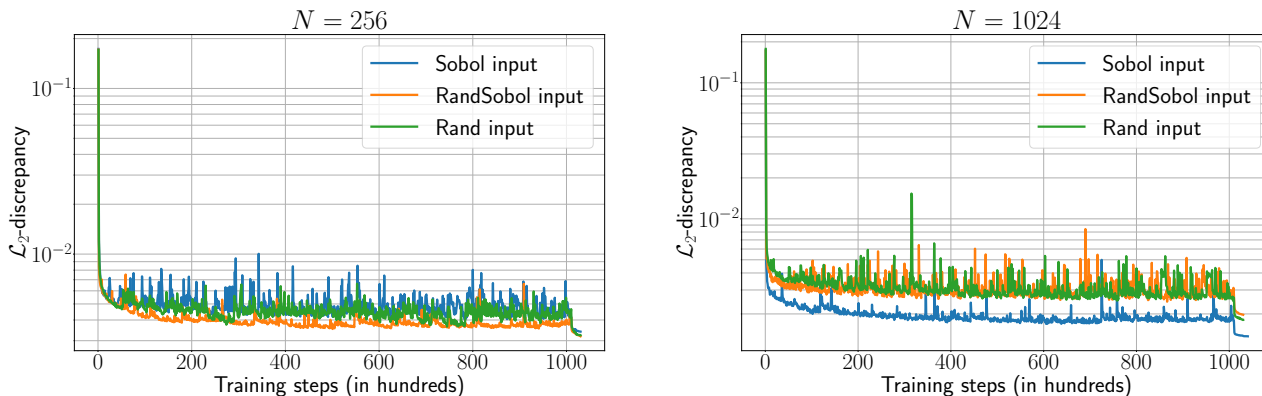


Figure 10. .

In the main text, we suggest three different input types to be transformed into low-discrepancy points via our MPMC framework, namely random points, Sobol', and randomized Sobol'. In this experiment, we empirically analyse how these different types influence the discrepancy of the resulting MPMC points. To this end, we train several MPMC models based on the three different input types and report the average \mathcal{L}_2 -discrepancy during training for two different number of points $N = 256, 1024$ in Fig. 10. We can see that on average either Sobol' or randomized Sobol' reach lower discrepancy values as well as exhibit faster convergence compared to random points. We note, however, that the single best MPMC model for each of the three different input point types yield almost identical discrepancy values. Thus, we conclude that Sobol' and randomized Sobol' points on average yield lower discrepancy values compared to random points, while at the same time the best performing input type has to be evaluated in practice for each number of points N .